INDIAN JOURNAL OF SCIENCE AND TECHNOLOGY

RESEARCH ARTICLE

Mathematical Simulation for MHD Casson Convective Nanofluid Flow Induced by 3D Permeable Sheet with Chemical Effect

Khyati Dang[1], Vinita Makkar[1]*, Naresh Sharma[1]

1 Department of Basic and Applied Sciences, SoES, GD Goenka University, Gurgaon, Haryana, India

OPEN ACCESS

Received: 16-01-2024

Accepted: 28-02-2024

Published: 19-04-2024

Citation: Dang K, Makkar V, Sharma N (2024) Mathematical Simulation for MHD Casson Convective Nanofluid Flow Induced by 3D Permeable Sheet with Chemical Effect. Indian Journal of Science and Technology 17(16): 1713-1723. https://doi.org/10.17485/IJST/v17i16.117

* **Corresponding author**.

vini252011makkar@gmail.com

Funding: None

Competing Interests: None

Published By Indian Society for Education and Environment (iSee)

ISSN
Print: 0974-6846
Electronic: 0974-5645

Abstract

Objectives: Current manuscript focuses on examination of chemical reaction and heat generation impacts on 3D MHD non-Newtonian nanofluid flow with convective boundary conditions induced by permeable sheet. Additionally, Brownian motion, non-Newtonian heating and thermophoretic processes as used for this study. **Methods:** A computational programme, MATLAB has been used for solving the system of O.D.Es with the help of ODE45 solver. The Runge Kutta Fehlberg approach is implemented to calculate the answer to the expression for temperature, velocity, and nanoparticle concentration after the shooting process. **Findings:** For a variety of fluid parameters, the temperature, concentration of nanoparticles, and dimensionless velocities are shown and examined, including permeability parameter $K_1\,(0.1 \leq K_1 \leq 0.4)$, magnetic $M(1.0 \leq M \leq 4.0)$, stretching ratio parameter $c(2.0 \leq c \leq 8.0)$, Lewis number $Le(1.0 \leq Le \leq 4.0)$, Brownian motion $Nb(1.0 \leq Nb \leq 4.0)$ and Prandtl number $Pr(0.2 \leq Pr \leq 0.8)$, thermal Biot number $t_b\,(0.1 \leq t_b \leq 0.7)$, Casson fluid parameter $\beta(0.2 \leq \beta \leq 0.8)$, chemical reaction parameter $c_h\,(1.0 \leq c_h \leq 4.0)$. The temperature is found to increase with an enhance in the thermal Biot number and to reduce with a greater Prandtl number and stretching ratio parameter. **Novelty:** Although the immense significance and frequent use of nanofluids in industries and technology, no effort has been made to explore the chemical influence on MHD Casson fluid flow using a three-dimensional permeable sheet. Through similarity transformations, the Runge-Kutta Fehlberg technique converts mass, momentum, and energy conservation equations into ODEs and incorporates boundary conditions. Skin friction and the heat transmission rate past an extending surface, which have an impact on technology and production, can be predicted using the results of this study.

Keywords: Chemical reaction; Buongiorno's model; Nanofluid; Biot numbers; 3D permeable sheet

1 Introduction

Many industries related to manufacturing grew in the early 20th century, such as substances and chemical compounds, petroleum and natural gas, beverages and food, fabric and the printing process, polyester extrusion, material for glass swaying, quickly apply cooling, microelectronics cooling, and extinction in metal manufacturing facilities, and refrigerant/lubricant mixtures to serve heating and cooling. These sectors are crucial, as are many others, including innovative and various fields such as cancer treatment, better surgery, heat pumps, and micro-channel thermal sinks. The concept of "nanofluid" is used to signify a mixture of various base fluids (e.g., liquids, gasoline, oil for engines, ethylene, and tri-ethylene alcohol) with nanoparticles (such as metallic substances, oxides, carbides, nitric oxide, and graphite fibers). Choi [(1)] was the first to undertake an experimental investigation and inform the researchers about the improvement of nanofluids' thermal conductivity. Ibrahim and Anbessa [(2)] discussed the Hall and Ion effects with varying slip circumstances in MHD nanofluid flow induced by 3D exponential sheet. 3D MHD flow generated by expanding surface with the impact of radiation in a porous medium using RKF technique has been evaluated by Mallikarjuna et al. [(3)]. Goyal et al. [(4)] discussed the triple diffusive effects along with regression analysis induced by power law extending surface employing the GFEM method.

The study of magnetohydrodynamics, or MHD, describes how a magnetic field affects a fluid. The fundamental idea of MHD is that fluid motion causes the magnetic field to produce forces that have the potential to induce magnetic induction. The crucial and inevitable benefits of MHD nano liquid movement and heat transport, such as rehabilitation, disinfection of equipment, stomach medicines, and significant roles in procedures like targeted drug release, cancer therapy, asthma treatment, immunological synergy, magnetically charged cell separation, MRI, and tumor elimination through overheating, especially among others. Arulmozhi et al. [(5)] investigated influence of energy and chemical process utilizing Roseland approximation along with comparative analysis. Cassini oval contained in porous medium influenced via Buoyancy effects in MHD nanofluid flow has been analyzed by Jalili et al. [(6)]. By using response surface technique, Hussain et al. [(7)] following SRM technique by considering Al_2O_3 water-based nanoparticles to investigate MHD nanofluid flow. By following FEM technique, Ali et al. [(8)] discussed the features of Cattaneo Christov utilizing MATLAB programming. By utilizing Buongiorno's model, Makkar et al. [(9)] addressed the influence of source of energy and chemical process influenced via nonNewtonian nanofluids in presence of heat radiation.

Because non-Newtonian fluids have so many uses in the chemical, petroleum, and engineering industries, researchers are very interested in studying them. Casson liquid is a special kind of non-Newtonian liquid with many uses in the food processing, metallurgy, drilling, and bioengineering industries, among other fields. Suresh et al. [(10)] studied Casson nanofluid circulation, heat, and transport of mass across an exponentially expanded surface. Investigation comprised the energy of stimulation, Hall voltage, radiant heat, thermal source/sink, thermophoresis, and Brownian motion. Ragupathi et al. [(11)] examined an analysis on the flow of a three-dimensional Casson nanofluid across an extended sheet. The study considered the impacts of the energy of Arrhenius activation and exponential sources of heat. A non-isothermal extending sheet has been studied by Ramesh et al. [(12)] for stagnation-point movement of an incompressible non-Newtonian liquid. Among two stationary porous disks, Madhukesh et al. [(13)] explored an unchanging, inflexible magnetic Casson-Maxwell non-Newtonian nanofluid. In a bidirectional nonlinear extending sheet, Puneeth et al. [(14)] explored the influence of mixed convection, Brownian motion, and thermophoresis on Casson hybrid nanofluid movements. For Casson and micropolar nanofluids, Ramesh et al. [(15)] studied inflexible, time-varying squeezing movement. Under gyrotactic bacteria on permeable surface, Madhukesh et al. [(16)] studied Marangoni convention Casson nanoliquid movement.

This research introduces a novel approach in the field of permeable extending surfaces. It utilizes the Runge-Kutta Fehlberg 45 procedure and a shooting technique to obtain numerical answers for the movement of a 3D MHD non-Newtonian liquid. The study also incorporates chemical reactions and heat generation. This analysis is based on appropriate graphs and numerical information presented in tables. The subsequent part presents the mathematical model and provides its explanations. The subsequent section outlines the suggested numerical methodology. Subsequently, the acquired outcomes are analyzed, incorporating visual depictions and their corresponding physical explanations. Lastly, the conclusions of the article are offered, emphasizing the most noteworthy findings achieved.

2 Methodology

Considered three-dimensional model comprises MHD movement of non-Newtonian nano liquid as well as heat generation and chemical reaction mixed in a porous sheet with heat and concentration Biot numbers. Figure 1 shows the physical depiction. At $\widehat{z} \geq 0$, flow is impeded and at $\widehat{z} = 0$, flow is situated among stretching velocities $U_w = a\widehat{x}\&V_w = b\widehat{y}$; where $a\&b$ are constants.

The governing equations are[17–19]:

$$\frac{\partial \hat{u}}{\partial \hat{x}}+\frac{\partial \hat{v}}{\partial \hat{y}}+\frac{\partial \hat{w}}{\partial \hat{z}}=0 \tag{1}$$

$$\hat{u}\frac{\partial \hat{u}}{\partial \hat{x}}+\hat{v}\frac{\partial \hat{u}}{\partial \hat{y}}+\hat{w}\frac{\partial \hat{u}}{\partial \hat{z}}=\nu\frac{\partial^2 \hat{u}}{\partial \hat{z}^2}-\left[\frac{\sigma B_0^2}{\rho}+\frac{\nu}{k_1}\left(1+\frac{1}{\beta}\right)\right]\hat{u}, \tag{2}$$

$$\hat{u}\frac{\partial \hat{v}}{\partial \hat{x}}+\hat{v}\frac{\partial \hat{v}}{\partial \hat{y}}+\hat{w}\frac{\partial \hat{v}}{\partial \hat{z}}=\nu\frac{\partial^2 \hat{v}}{\partial \hat{z}^2}-\left[\frac{\sigma B_0^2}{\rho}+\frac{\nu}{k_1}\left(1+\frac{1}{\beta}\right)\right]\hat{v}, \tag{3}$$

$$\hat{u}\frac{\partial \hat{T}}{\partial \hat{x}}+\hat{v}\frac{\partial \hat{T}}{\partial \hat{y}}+\hat{w}\frac{\partial \hat{T}}{\partial \hat{z}}=\frac{k}{(\rho C_p)_f}\frac{\partial^2 \hat{T}}{\partial \hat{z}^2}+\frac{(\rho C_p)_p}{(\rho C_p)_f}\left[\frac{D_T}{T_\infty}\left(\frac{\partial \hat{T}}{\partial \hat{z}}\right)^2+D_B\frac{\partial \hat{T}}{\partial \hat{z}}\frac{\partial \hat{C}}{\partial \hat{z}}\right]-\frac{1}{(\rho C_p)_f}\frac{\partial q_r}{\partial \hat{z}} \tag{4}$$

$$\hat{u}\frac{\partial \hat{C}}{\partial \hat{x}}+\hat{v}\frac{\partial \hat{C}}{\partial \hat{y}}+\hat{w}\frac{\partial \hat{C}}{\partial \hat{z}}=\frac{D_T}{\hat{T}_\infty}\frac{\partial^2 \hat{T}}{\partial \hat{z}^2}+D_B\frac{\partial^2 \hat{C}}{\partial \hat{z}^2}-K_r\left(\hat{C}-\hat{C}_\infty\right) \tag{5}$$

The various elements of velocity across the $\hat{x},\hat{y}$ and $\hat{z}$ axes are indicated through $\hat{u},\hat{v}$ and $\hat{w}$ in preceding equation. $\hat{C}$ denotes the fluid concentration, ρ stand for fluid density, $\hat{T}$ denotes the fluid temperature, ν stands for kinematic viscosity, k denotes the permeability, K_r denotes the chemical reaction parameter, D_B designates the Brownian motion, D_T designates the coefficient of thermophoresis diffusion and C_p represents the specific heat capacity.

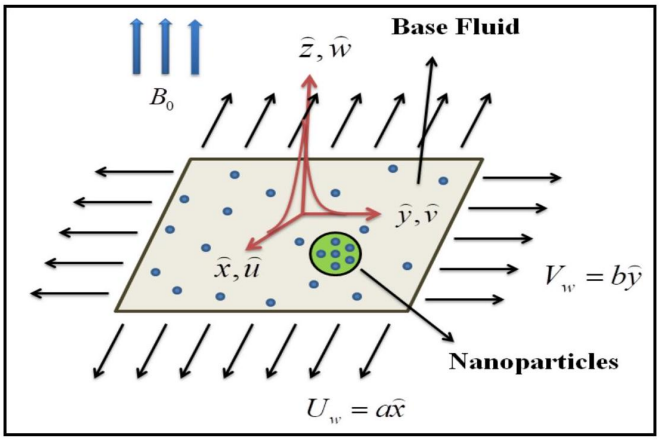

Fig 1. Physical diagram

where $\hat{T}_\infty$ denotes the ambient temperature, $\hat{T}_w$ designates the surface temperature, $\hat{C}_\infty$ stand for ambient concentration and $\hat{C}_w$ denotes the nanoparticle concentration at the surface, appropriately, where wall temperature is greater than ambient temperature.

Using similarity variables[20] :

$$\eta=\sqrt{\frac{a}{\nu}}\hat{z},\ \Theta(\eta)=\frac{\hat{T}-\hat{T}_\infty}{\hat{T}_w-\hat{T}_\infty},\ \Phi(\eta)=\frac{\hat{C}-\hat{C}_\infty}{\hat{C}_w-\hat{C}_\infty},\ \hat{u}=a\hat{x}f'(\eta),\ \hat{v}=b\hat{y}g'(\eta)$$
$$and\ \hat{w}=-\sqrt{a\nu}[f(\eta)+cg(\eta)] \tag{6}$$

Associated B.C's are:

$$\begin{aligned}&\widehat{u}=U_w=a\widehat{x},\quad \widehat{v}=V_w=b\widehat{y}\quad \text{at}\quad \widehat{w}=0\\&-k_f\left(\frac{\partial\widehat{T}}{\partial\widehat{z}}\right)=h_f\left(\widehat{T}_w-\widehat{T}\right),\quad -D_B\left(\frac{\partial\widehat{C}}{\partial\widehat{z}}\right)=h_s\left(\widehat{C}_w-\widehat{C}\right)\quad \text{at}\quad \widehat{z}=0\\&\widehat{u}\to 0,\quad \widehat{v}\to 0,\quad \widehat{T}\to\widehat{T}_\infty,\quad \widehat{C}\to\widehat{C}_\infty\quad \text{as}\quad \widehat{z}\to\infty\end{aligned}\tag{7}$$

Final transformed D.E's are:

$$\left(1+\frac{1}{\beta}\right)f'''-f'^2+(f+cg)f''-\left[M+K_1\left(1+\frac{1}{\beta}\right)\right]f'=0\tag{8}$$

$$\left(1+\frac{1}{\beta}\right)g'''-cg'^2+(f+cg)g''-\left[M+K_1\left(1+\frac{1}{\beta}\right)\right]g'=0\tag{9}$$

$$\Theta''+Pr\left((f+cg)\Theta'+Nb\Theta'\Phi'+Nt\Theta'^2+Q\Theta\right]=0\tag{10}$$

$$\Phi''+LePr(f+cg)\Phi'+\left(\frac{Nt}{Nb}\right)\Theta''-LePrC_h\Phi=0\tag{11}$$

Reduced B.C's are:

$$\begin{aligned}&f'=1,\quad g'=1,\quad \Theta'(\xi)=-t_b(1-\Theta(\xi)),\quad \Phi'(\xi)=-c_b(1-\Phi(\xi)),\\&f'\to 0,\quad g'\to 0,\quad \Theta\to 0,\quad \Phi\to 0\end{aligned}\tag{12}$$

where dashes denote the differentiation about ξ and Pr denotes the Prandtl number, Le denotes the Lewis number, β designates the parameter of Casson fluid, t_b denotes thermal Biot number, Nt stands for the parameter of thermophoresis, c_b stands for concentration Biot number, M denotes the parameter of magnetic, and Nb denotes the Brownian motion parameter described in the following way:

$$\begin{aligned}&\beta=\frac{\mu_B}{p_z}\sqrt{2\pi_c},\ M=\frac{\sigma {B_0}^2}{a\rho},\ Pr=\frac{\nu\rho C_p}{k},\ Nb=\frac{\tau D_B\left(\widehat{C}_w-\widehat{C}_\infty\right)}{\nu},\\&Le=\frac{\alpha}{D_B},\ Nt=\frac{\tau D_T\left(\widehat{T}_w-\widehat{T}_\infty\right)}{\nu\widehat{T}_\infty},\ t_b=\frac{h_f}{\sqrt{\frac{a}{\nu}k_f}},\ c_b=\frac{h_s}{\sqrt{\frac{a}{\nu}D_B}}\end{aligned}\tag{13}$$

Dimensionless representations of physical quantities are:

$$Sh_x=\frac{-\widehat{x}}{\left(\widehat{C}_w-\widehat{C}_\infty\right)}\left(\frac{\partial\widehat{C}}{\partial\widehat{z}}\right)|_{\overline{z}=0},\ Nu_x=\frac{-\widehat{x}}{\left(\widehat{T}_w-\widehat{T}_\infty\right)}\left(\frac{\partial\widehat{T}}{\partial\widehat{z}}\right)|_{\overline{z}=0},\ Cf_y=\frac{\tau_{yz}}{\rho {U_w}^2}\ and\ Cf_x=\frac{\tau_{xz}}{\rho {U_w}^2}\tag{14}$$

$$Sh_{\hat{x}}\mathrm{Re}_{\hat{x}}^{-1/2}=-\Phi'(0),Nu_{\hat{x}}\mathrm{Re}_{\hat{x}}^{-1/2}=-\Theta'(0),Cf_{\hat{y}}\mathrm{Re}_{\hat{x}}^{1/2}=\left(1+\frac{1}{\beta}\right)g''(0)\quad \text{and}\quad Cf_{\hat{x}}\mathrm{Re}_{\hat{x}}^{1/2}=\left(1+\frac{1}{\beta}\right)f''(0)\tag{15}$$

Here Sh_x denotes Sherwood number, Nu_x stands for Nusselt number, Cf_y&Cf_x denotes skin friction coefficient in y&x directions. Re_x is local Reynolds number.

2.1 Numerical Scheme

In order to acquire numerical solutions, the step size is constrained to 0.01 and the maximum value is set to 10. The Shooting technique is superior than other numerical methods due to its fifth-order truncation error. It is also easier to calculate the solution than other numerical approaches. Using the RKF process and the ODE45 solver in MATLAB R2014a, the arrangement of D.E.'s Equations (8), (9), (10) and (11) with B. C's Equation (12) is mathematically handled. These conditions are then converted into ten first order D. E's as

$$\widetilde{o}(1)^{'} = \widetilde{o}(2) \tag{16}$$

$$\widetilde{o}(2)^{'} = \widetilde{o}(3) \tag{17}$$

$$\widetilde{o}(3)^{'} = \frac{\beta}{(1+\beta)}\left[\widetilde{o}(2)^2 - \{\widetilde{o}(1) + \widetilde{co}(4)\}\widetilde{o}(3) + M\widetilde{o}(2) + K_1\left(1+\frac{1}{\beta}\right)\widetilde{o}(2)\right] \tag{18}$$

$$\widetilde{o}(4)^{'} = \widetilde{o}(5) \tag{19}$$

$$\widetilde{o}(5)^{'} = \widetilde{o}(6) \tag{20}$$

$$\widetilde{o}(6)^{'} = \frac{\beta}{(1+\beta)}\left[\widetilde{cO}(5)^2 - \{\widetilde{O}(1) + \widetilde{co}(4)\}\widetilde{o}(6) + M\widetilde{o}(5) + \beta K_1\left(1+\frac{1}{\beta}\right)\widetilde{o}(5)\right] \tag{21}$$

$$\widetilde{o}(7)^{'} = \widetilde{o}(8) \tag{22}$$

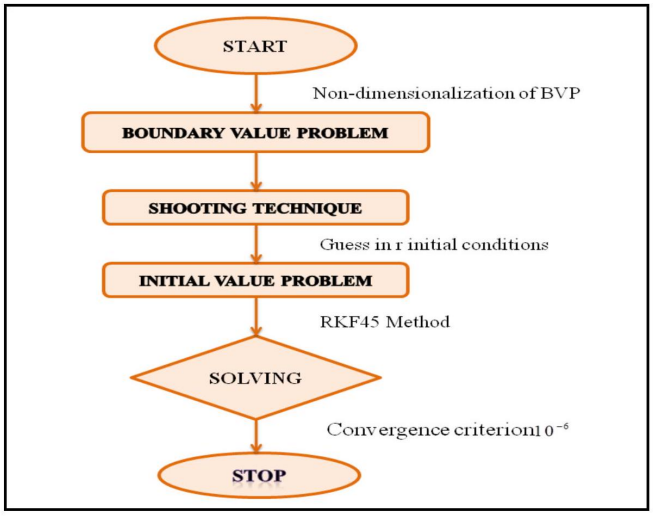

Fig 2. Flow chart (Shooting technique)

$$\widetilde{o}(8)^{'} = -Pr\left[\{\widetilde{o}(1) + \widetilde{co}(4)\}\widetilde{o}(8) + Nb\widetilde{o}(8)\widetilde{o}(10) + Nt\widetilde{o}(8)^2\right] \tag{23}$$

$$\widetilde{o}(9)' = \widetilde{o}(10) \tag{24}$$

$$\widetilde{o}(10)' = -LePr\{\widetilde{o}(1) + \widetilde{co}(4)\}\widetilde{o}(10) - \left(\frac{Nt}{Nb}\right)\widetilde{o}(8)' \tag{25}$$

where,

$$\begin{aligned} &f = \widetilde{o}(1),\ f' = \widetilde{o}(2),\ f'' = \widetilde{o}(3),\ f''' = \widetilde{o}(3)' \\ &g = \widetilde{o}(4),\ g' = \widetilde{o}(5),\ g'' = \widetilde{o}(6),\ g''' = \widetilde{o}(6)' \\ &\Theta = \widetilde{o}(7),\ \Theta' = \widetilde{o}(8),\ \Theta'' = \widetilde{o}(8)' \\ &\Phi = \widetilde{o}(9),\ \Phi' = \widetilde{o}(10),\ \Phi'' = \widetilde{o}(10)' \end{aligned} \tag{26}$$

3 Results and Discussion

In results and discussion part, tables and graphs are produced by MATLAB programming that adheres to the RKF method and uses the shooting algorithm. Table 1 addresses results are compared for different Pr with Nadeem & Hussain et al.[21], Mankinde and Aziz[22] and Mabood et al.[23] along with residual error.Table 2 illustrates values of $f''(0)\&g''(0)$ for different β, K_1 and M. Table 3 shows values of $-\Theta'(0)$ for different t_b, c, Pr and Q. Table 4 shows values of $-\Phi'(0)$ for different c_b, Le, Nb and c_h.

Table 1. Comparison of results for different Pr with Hussain et al.[21], Makinde and Aziz[22] and Mabood et al.[23] along with residual error

Pr	Nadeem & Hussain[21]	Residual error	Mankinde and Aziz[22]	Residual error	Mabood et al.[23]	Residual error	Present result
2	0.911	-0.0004	0.9114	0.0000	0.9114	0.0000	0.9114
20	-	-	-	-	3.3539	0.0000	3.3539
70	-	-	-	-	6.4622	0.0000	6.4622

Table 2. Values of $f''(0)\&g''(0)$ for different β, K_1 and M

β	K_1	M	$f''(0)$	$g''(0)$
0.2	0.1	1.5	-0.795438997570700	-0.862266383279772
0.4	-	-	-1.006891311142385	-1.097115497396029
0.6	-	-	-1.140037893261985	-1.244509161174477
0.8	-	-	-1.233703833454660	-1.348054410136592
0.1	0.1	-	-0.624727280196918	-0.671375151909698
-	0.2	-	-0.699843393413229	-0.741817920658436
-	0.3	-	-0.767758999806563	-0.806222825242935
-	0.4	-	-0.830194848542521	-0.865899477591088
-	0.1	1.0	-0.587505650247634	-0.636853775397441
-	-	2.0	-0.659908803333436	-0.704250292235119
-	-	3.0	-0.725265977898990	-0.765856344335151
-	-	4.0	-0.785274633517415	-0.822923495273280

Table 3. Values of $-\Theta'(0)$ for different t_b, c, Pr and Q

t_b	c	Pr	Q	$-\Theta'(0)$
0.1	2.0	0.7	0.5	0.089039205765280
0.3	-	-	-	0.217101784005240
0.5	-	-	-	0.302783717173519
0.7	-	-	-	0.363192593091559

Continued on next page

Table 3 continued

0.3	2.0	-	-	0.217101784005240
-	4.0	-	-	0.237617338613509
-	6.0	-	-	0.247510825975642
-	8.0	-	-	0.253688746202321
-	2.0	0.2	-	0.156717457123504
-	-	0.4	-	0.194508918188927
-	-	0.6	-	0.211440778932070
-	-	0.8	-	0.221698735155712
-	-	0.7	0.0	0.228925653259389
-	-	-	0.5	0.217101784005240
-	-	-	1.0	0.195947901900813
-	-	-	1.5	0.139687026785950

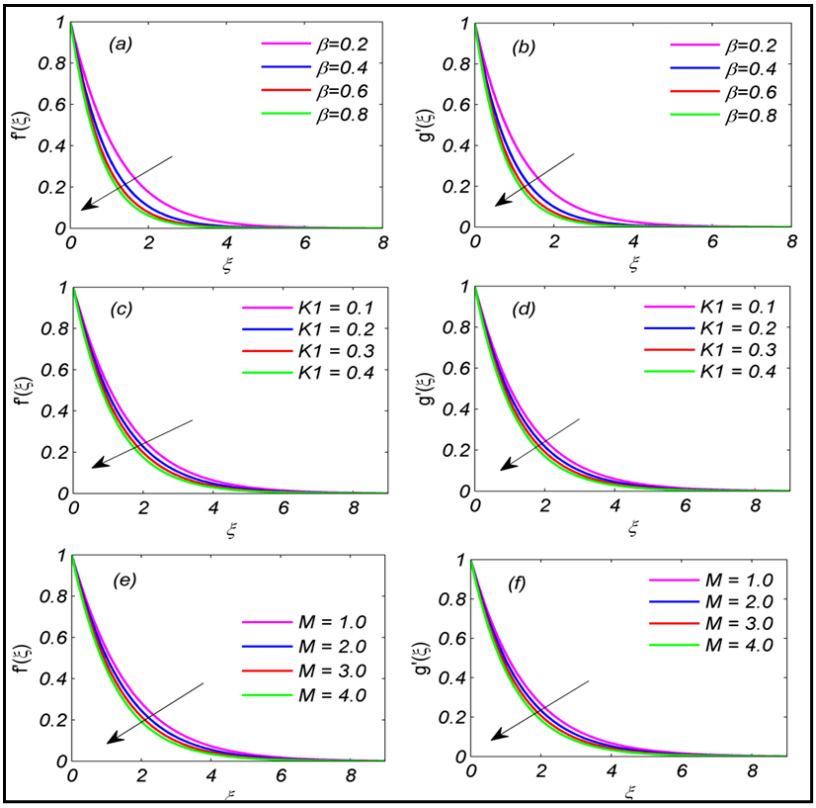

Fig 3. Axial and transverse velocity profile for (a, b)β, (c, d) K_1 and (e, f) M

Figure 3 manifests impact of axial and transverse velocity distribution against Casson fluid parameter β, permeability parameter K_1 and parameter of magnetic M. Figure 3**(a)** and **(b)** exhibits influence of axial velocity $f^{'}(\xi)$ and transverse velocity $g^{'}(\xi)$ against Casson fluid parameter β in the range $0.2 \leq \beta \leq 0.8$. It is found that higher β produces sheer stress that simultaneously falls down velocity distribution as visualized in Figure 3**(a)** and **(b)**. Figure 3**(c)** and **(d)** manipulates the effects of $f^{'}(\xi)$ and $g^{'}(\xi)$ against permeability parameter K_1 $(0.1 \leq K_1 \leq 0.4)$. Velocity profile decreases in both the cases as noticed in both the Figure 3**(c)** and **(d)** respectively and simultaneously skin friction along x&y direction falls down. Figure 3**(e)** and **(f)** shows axial and transverse velocity distribution under the consequence of magnetic parameter $M(1.0 \leq M \leq 4.0)$. Due to presence of magnetism, Lorentz force produces, thusly velocity escalates as shown via Figure 3 **(e)** and **(f)** serially.

Figure 4**(a)**-**(d)** manifests the influence of distribution of temperature against fluid parameters t_b (thermal Biot number), c (stretching ratio parameter), Pr (Prandtl number) and Q (heat generation parameter) respectively. Figure 4**(a)** presents graphs for $\Theta(\xi)$ against t_b in the range $0.1 \leq t_b \leq 0.7$. This plot shows augmentation in temperature distribution with augmentation in

Table 4. Values of $-\Phi'(0)$ for different c_b, Le, Nb and c_h

c_b	Le	Nb	c_h	$-\Phi'(0)$
1.0	2.0	0.1	0.7	0.528429129081087
3.0	-	-	-	0.925995503657038
5.0	-	-	-	1.090020721434213
7.0	-	-	-	1.179569699941275
0.1	1.0	-	-	0.060212616290614
-	2.0	-	-	0.077757989232873
-	3.0	-	-	0.084354751259548
-	4.0	-	-	0.087854311390063
-	2.0	0.1	-	0.077757989232873
-	-	0.2	-	0.086259452003076
-	-	0.3	-	0.089093320857230
-	-	0.4	-	0.090510290289214
-	-	0.1	1.0	0.080714403892159
-	-	-	2.0	0.087067836209325
-	-	-	3.0	0.090574272038795
-	-	-	4.0	0.092725041464002

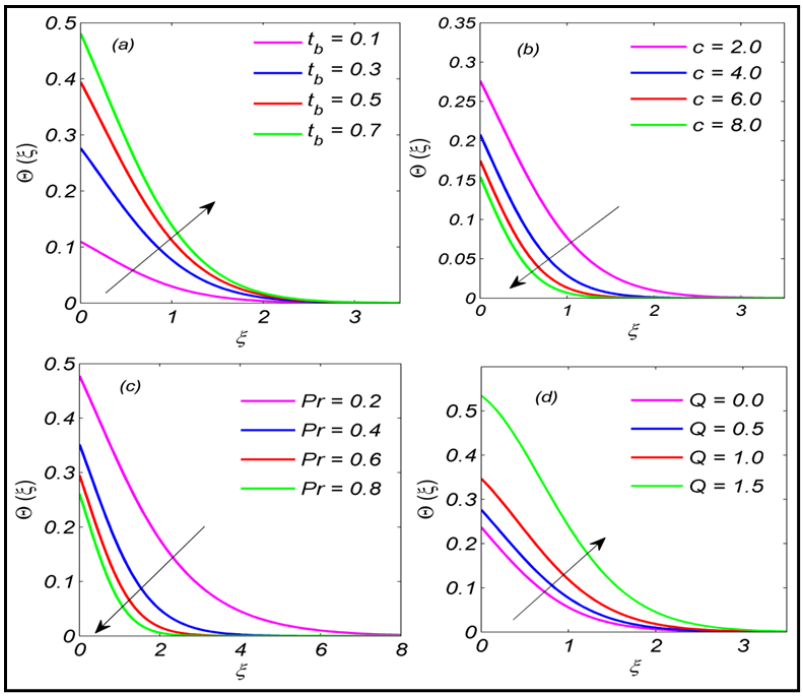

Fig 4. Temperature distribution for (a)t_b, (b) c, (c) Pr and (d) Q

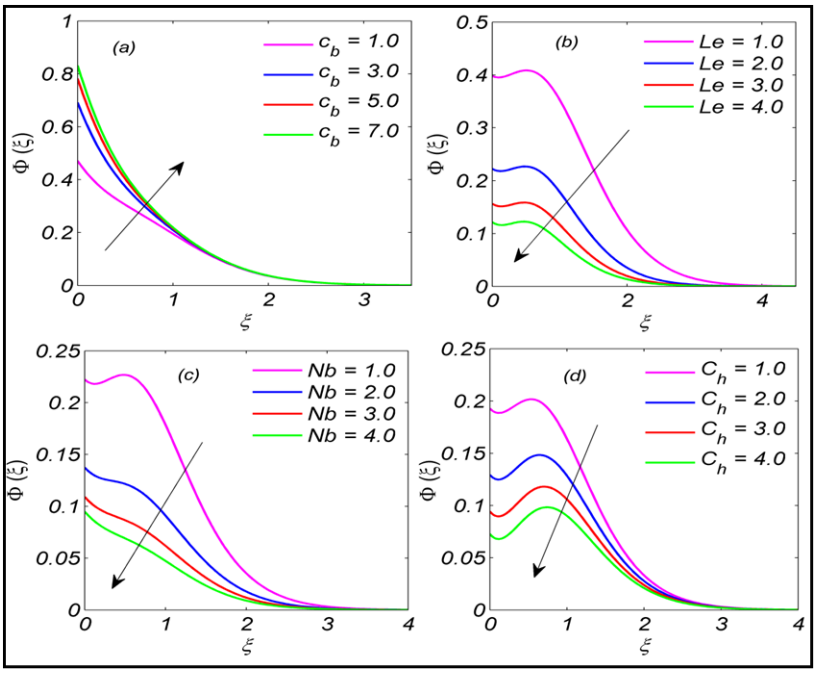

Fig 5. Concentration profile for (a)c_b, (b) Le,(c) Nb and (d) c_h

t_b (thermal Biot number). As the Biot number rises, the fluid's resistance drops, leading to an upsurge in temperature. Impact of temperature distribution against c (stretching ratio parameter) has been displayed via Figure 4**(b)**. It is found that higher $c(2.0 \leq c \leq 8.0)$, values of $\Theta(\xi)$ falls down as visualized in Figure 4**(b)**. Figure 4**(c)** manifest impact of $\Theta(\xi)$ under the influence of Pr (Prandtl number) within the range $0.2 \leq Pr \leq 0.8$. With increase in Pr, a drop in the values of temperature distribution has been determined as shown in Figure 4**(c)** and it turns out that the distribution of energy drops. A lower Prandtl number in a liquid state reduces thermal conductivity which results enhance in the rate of energy transmission. Figure 4 **(d)** shows influence of heat generation parameter Q in the range $0.0 \leq Q \leq 1.5$ (i.e., in the absence and presence of heat generation) over nanoparticle temperature distribution and it is found that temperature enhances with higher Q. The formation of heat occurs when the value of Q is positive, whereas the absorption of heat occurs when the value of Q is negative. An external heat supply is responsible for producing the heat that causes the temperature to rise.

Figure 5**(a)**-**(d)** presents the influence of concentration profile against fluid parameters concentration Biot number c_b, Lewis number Le, Brownian motion Nb and chemical reaction c_h respectively. In Figure 5**(a)**, with rise in concentration Biot number $c_b\,(1.0 \leq c_b \leq 7.0)$, concentration distribution rises. A bigger Biot number results in a higher concentration since it improves the heating region. Figure 5**(b)** manifests concentration profile against Lewis number Le. It is found that, augmentation in Le in the range $1.0 \leq Le \leq 4.0$ falls down concentration distribution. Influence of Brownian motion $Nb(1.0 \leq Nb \leq 4.0)$ over nanoparticle concentration has been visualized in Figure 5**(c)**. The results show that the concentration profile and thickness of boundary layer are both reduced when the Brownian motion value increases. As the mass label grows, the Brownian motion flow rate drops. Figure 5**(d)** shows impact of $\Phi(\xi)$ under the influence of c_h (Chemical reaction parameter) in the range $c_h\,(1.0 \leq c_h \leq 4.0)$. According to the facts, both are inversely proportional, which means that the concentration profile falls as the c_h value rises. Figure 6**(a)**-**(d)** shows the influence of skin friction coefficient against t_b&c, c&c_b, c&Nt, and c&Pr respectively via contour plots. Figure 6**(a)** manifests skin friction against thermal Biot number $t_b\,(1.25 \leq t_b \leq 1.50)$ and stretching ratio parameter $c(1.25 \leq c \leq 1.50)$ and it has been noticed via this contour plot that with increase in both t_b&c, skin friction rises up as visualized in this contour plot. Figure 6**(b)** presents contour plot of skin friction over $c(1.35 \leq c \leq 1.45)$ and $c_b\,(1.35 \leq c_b \leq 1.45)$ and it manifests that skin friction falls down with rise in both c&c_b. In a similar way, Figure 6**(c)** and **(d)** show same impact as of Figure 6**(b)**. Both the contour plots of skin friction show that skin friction declines with higher $c(1.25 \leq c \leq 1.50)$&$(1.25 \leq Nt \leq 1.50)$ and $c(1.40 \leq c \leq 1.50)$&$Pr(1.40 \leq Pr \leq 1.50)$ respectively as visualized in Figure 6 **(c)** and **(d)**.

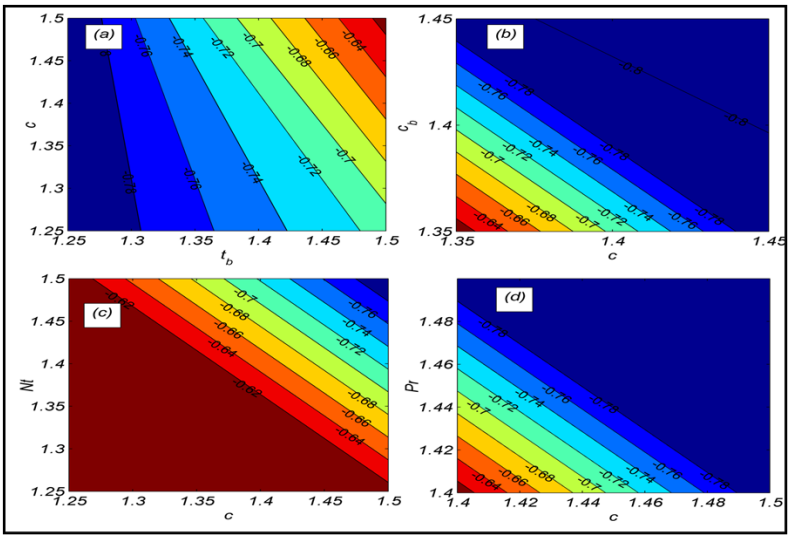

Fig 6. Skin friction coefficient against (a)t_b&c, (b) c&c_b, (c) c&Nt, and (d) c&Pr

4 Conclusion

The present study examines the radiation, mass, and mobility transmission of magnetohydrodynamic (MHD) Casson nano liquids with convective boundary circumstances on a three-dimensional permeable sheet. The current study's findings include the significance of chemical process and heat generation impacts, the profile of the flow velocity of the MHD Casson fluid, the distribution of temperatures, and the nanoparticle concentration. The latest study is summarized by the following key findings:

- Skin friction coefficient falls down for permeability parameter $K_1\,(0.1 \leq K_1 \leq 0.4)$ while rises up for Casson fluid parameter $\beta\,(0.2 \leq \beta \leq 0.8)$ due to produced shear stress.
- Velocity profile escalates down for Magnetic parameter $M(1.0 \leq M \leq 4.0)$ due to produced Lorentz drag force when rises in the value of M.
- Higher value of thermal Biot number t_b and heat generation parameter Q augmented temperature distribution while opposite trend is observed for c and Pr.
- With increase in both c (stretching ratio parameter) and c_b (concentration Biot number), skin friction coefficient escalates.
- Concentration mounted for concentration Biot number c_b while declines for greater chemical reaction parameter c_h.

Over stretched surfaces, it is intended that the current study will act as a catalyst for the development of technical applications among researchers. It is quite tough to hit and award an initial approximation in shooting method. As a consequence of this, the step is time-consuming. It is possible to extend this comparison to include Cattaneo-Christov heat flow, changing sheet thickness, and melting heat transfer.

References

1) Choi SUS, Eastman JA. Enhancing thermal conductivity of fluids with nanoparticles. In: Argonne National Lab. (ANL), Argonne, IL (United States). 1995. Available from: https://www.osti.gov/biblio/196525.
2) Ibrahim W, Anbessa T. Three-Dimensional MHD Mixed Convection Flow of Casson Nanofluid with Hall and Ion Slip Effects. *Mathematical Problems in Engineering*. 2020;2020:1–15. Available from: https://doi.org/10.1155/2020/8656147.
3) Mallikarjuna HB, Jayaprakash MC, Mishra R. Three-Dimensional Boundary layer Flow and Heat Transfer of a Fluid Particle Suspension over a Stretching Sheet Embedded in a Porous Medium. *Nonlinear Engineering*. 2019;8(1):734–743. Available from: https://doi.org/10.1515/nleng-2018-0008.
4) Goyal R, Vinita, Sharma N, Bhargava R. GFEM analysis of MHD nanofluid flow toward a power-law stretching sheet in the presence of thermodiffusive effect along with regression investigation. *Heat Transfer*. 2021;50(1):234–256. Available from: https://doi.org/10.1002/htj.21873.
5) Arulmozhi S, Sukkiramathi K, Santra SS, Edwan R, Fernandez-Gamiz U, Noeiaghdam S. Heat and mass transfer analysis of radiative and chemical reactive effects on MHD nanofluid over an infinite moving vertical plate. *Results in Engineering*. 2022;14:100394. Available from: https://doi.org/10.1016/j.rineng.2022.100394.
6) Jalili B, Sadighi S, Jalili P, Ganji DD. Numerical analysis of MHD nanofluid flow and heat transfer in a circular porous medium containing a Cassini oval under the influence of the Lorentz and buoyancy forces. *Heat Transfer*. 2022;51(7):6122–6138. Available from: https://doi.org/10.1002/htj.22582.
7) Hussain S, Rasheed K, Ali A, Vrinceanu N, Alshehri A, Shah Z. A sensitivity analysis of MHD nanofluid flow across an exponentially stretched surface with non-uniform heat flux by response surface methodology. *Scientific Reports*. 2022;12(1):1–17. Available from: https://doi.org/10.1038/s41598-022-22970-y.

8) Ali L, Ali B, Ghori MB. Melting effect on Cattaneo–Christov and thermal radiation features for aligned MHD nanofluid flow comprising microorganisms to leading edge: FEM approach. *Computers & Mathematics with Applications*. 2022;109:260–269. Available from: https://doi.org/10.1016/j.camwa.2022.01.009.
9) Makkar V, Poply V, Sharma N. Radiative MHD Non-Newtonian Chemically Reactive Nanofluid Flow with Heat Source Induced by Non-linear Stretching Cylinder. *Trends in Sciences*. 2022;19(21):1–21. Available from: https://doi.org/10.48048/tis.2022.6314.
10) Kumar YS, Hussain S, Raghunath K, Ali F, Guedri K, Eldin SM, et al. Numerical analysis of magnetohydrodynamics Casson nanofluid flow with activation energy, Hall current and thermal radiation. *Scientific Reports*. 2023;13(1):1–19. Available from: https://doi.org/10.1038/s41598-023-28379-5.
11) Ragupathi P, Saranya S, Mittal HVR, Al-Mdallal QM. Computational Study on Three-Dimensional Convective Casson Nanofluid Flow past a Stretching Sheet with Arrhenius Activation Energy and Exponential Heat Source Effects. *Complexity*. 2021;2021:1–16. Available from: https://doi.org/10.1155/2021/5058751.
12) Ramesh GK, Prasannakumara BC, Gireesha BJ, Rashidi MM. Casson Fluid Flow near the Stagnation Point over a Stretching Sheet with Variable Thickness and Radiation. *Journal of Applied Fluid Mechanics*. 2016;9(3):1115–1122. Available from: https://www.jafmonline.net/article_1689_d30bc2af3cee1df95fb95965d92ae990.pdf.
13) Madhukesh JK, Ramesh GK, Shehzad SA, Chapi S, Kushalappa IP. Thermal transport of MHD Casson–Maxwell nanofluid between two porous disks with Cattaneo–Christov theory. *Numerical Heat Transfer, Part A: Applications*. 2023. Available from: https://doi.org/10.1080/10407782.2023.2214322.
14) Puneeth V, Manjunatha S, Madhukesh JK, Ramesh GK. Three dimensional mixed convection flow of hybrid casson nanofluid past a non-linear stretching surface: A modified Buongiorno's model aspects. *Chaos, Solitons & Fractals*. 2021;152:111428. Available from: https://doi.org/10.1016/j.chaos.2021.111428.
15) Ramesh GK, Roopa GS, Rauf A, Shehzad SA, Abbasi FM. Time-dependent squeezing flow of Casson-micropolar nanofluid with injection/suction and slip effects. *International Communications in Heat and Mass Transfer*. 2021;126:105470. Available from: https://doi.org/10.1016/j.icheatmasstransfer.2021.105470.
16) Madhukesh JK, Ramesh GK, Prasannakumara BC, Shehzad SA, Abbasi FM. Bio-Marangoni convection flow of Casson nanoliquid through a porous medium in the presence of chemically reactive activation energy. *Applied Mathematics and Mechanics*. 2021;42(8):1191–1204. Available from: https://doi.org/10.1007/s10483-021-2753-7.
17) Buongiorno J. Convective Transport in Nanofluids. *Journal of Heat Transfer*. 2006;128(3):240–250. Available from: https://doi.org/10.1115/1.2150834.
18) Shateyi S. Numerical Analysis of Three-Dimensional MHD Nanofluid Flow over a Stretching Sheet with Convective Boundary Conditions through a Porous Medium. In: Kandelousi MS, editor. Nanofluid Heat and Mass Transfer in Engineering Problems. InTech. 2017. Available from: https://www.intechopen.com/chapters/52694.
19) Khan JA, Mustafa M, Hayat T, Alsaedi A. Three-dimensional flow of nanofluid over a non-linearly stretching sheet: An application to solar energy. *International Journal of Heat and Mass Transfer*. 2015;86:158–164. Available from: https://doi.org/10.1016/j.ijheatmasstransfer.2015.02.078.
20) Sulochana C, Ashwinkumar GP, Sandeep N. Similarity solution of 3D Casson nanofluid flow over a stretching sheet with convective boundary conditions. *Journal of the Nigerian Mathematical Society*. 2016;35(1):128–141. Available from: https://doi.org/10.1016/j.jnnms.2016.01.001.
21) Nadeem S, Hussain ST. Flow and heat transfer analysis of Williamson nanofluid. *Applied Nanoscience*. 2014;4(8):1005–1012. Available from: https://doi.org/10.1007/s13204-013-0282-1.
22) Makinde OD, Aziz A. Boundary layer flow of a nanofluid past a stretching sheet with a convective boundary condition. *International Journal of Thermal Sciences*. 2011;50(7):1326–1332. Available from: https://doi.org/10.1016/j.ijthermalsci.2011.02.019.
23) Mabood F, Khan WA, Ismail AIM. MHD boundary layer flow and heat transfer of nanofluids over a nonlinear stretching sheet: A numerical study. *Journal of Magnetism and Magnetic Materials*. 2015;374:569–576. Available from: https://doi.org/10.1016/j.jmmm.2014.09.013.